THESIS TITLE

by

Kara Kundert

A thesis submitted in partial satisfaction of the

requirements for the degree of

Master of Astrophysics

in

Astronomy

in the

Graduate Division

of the

University of California, Berkeley

Committee in charge:

Professor Aaron Parsons, Chair
Professor Martin White
Professor TBD

Fall 2018

The thesis of Kara Kundert, titled THESIS TITLE, is approved:

Chair _____ Date _____

_____ Date _____

_____ Date _____

University of California, Berkeley

THESIS TITLE

Abstract

THESIS TITLE

by

Kara Kundert

Master of Astrophysics in Astronomy

University of California, Berkeley

Professor Aaron Parsons, Chair

In this memo, we seek to lay out a case for the use of absorber in an interferometric study of the spatial monopole of the 21cm reionization signature (i.e. the "global signal"). As discussed in previous memos, we believe that the way to optimize the sensitivity to the monopole term comes from the use of absorptive walls between the antennas to impose an artificially high "horizon", or temperature discontinuity, onto the beam of each antenna, thereby pushing the monopole into higher order spatial terms (Kundert 2016). With the new simulation, we are able to manipulate many parameters of our virtual interferometer, including but not limited to the antenna spacing, absorber wall height, and the attenuating properties of the absorber itself. From our exploration of these parameters, we are able to now state with certainty that we are able to detect the monopole term of the sky using a classical interferometer.

To DEDICATED PERSON

This is the dedication.

Contents

Contents **ii**

List of Figures **iii**

List of Tables **iv**

1 Introduction **1**

2 The Global Signal – Its Physics and Significance to Cosmology **2**
2.1 Overview of the Epoch of Reionization 2
2.2 Overview of the Global Signal 3

3 Interferometry **6**
3.1 Brief Overview 6
3.2 Spatial Modes and Interferometric Sensitivities 6
3.3 Observing the Spatial Monopole with an Interferometer 6

4 Absorber – A New Approach to Monopole Interferometry **7**
4.1 Practical Instrumentation 7
4.2 Manipulating the Spatial Monopole 7
4.3 Initial Results 7

5 Overview of the Theory of HYPERION **8**
5.1 Simulation 8

6 Sensitivity to the Monopole Sky **11**
6.1 Simulated 11
6.2 Recovered 11

7 Conclusion **14**

Bibliography **15**

List of Figures

2.1 In the top half of the figure, we see a cartoon of the reionization history of the universe and the development and growth of ionized bubbles over time. In the bottom half, we see a breakdown of T_b, the brightness temperature of the 21 cm global signal, over time. There are five labeled regimes to this plot, each corresponding to the dominance of a different variable in the production of the 21 cm signal. Figure originally published in Pritchard & Loeb 2012. 4

6.1 Shown here is the absolute value of the visibility of a spectrally flat monopole sky with no absorber walls versus frequency. As can be seen already, the interferometer does have non-zero sensitivity to the monopole, though it is plainly clear that the autocorrelation term (shown in blue) is more sensitive than any of the non-zero interferometric baseline pairings. 12

6.2 REMAKE THIS FIGURE Shown here is the absolute value of the visibility of a spectrally flat monopole sky with no absorber walls versus uv-baseline. As can be seen already, the interferometer has a non-zero sensitivity to the monopole at non-zero baseline separations. 13

List of Tables

Acknowledgments

These are the acknowledgements.

Chapter 1

Introduction

very quick overview of HYPERION and breakdown of what's in each chapter

Chapter 2

The Global Signal – Its Physics and Significance to Cosmology

2.1 Overview of the Epoch of Reionization

In brief, the Epoch of Reionization refers to the period of the universe's history during which its supply of intergalactic hydrogen became reionized. This is important to its evolution, and therefore of interest to astronomers, due to the driving factor of that ionization: the ignition of the first stars, galaxies, and black holes in the universe. A positive detection of the Epoch of Reionization will help astronomers to clarify many open questions of cosmology, such as the properties of the first galaxies, how stars with zero metallicity formed, the physics of early quasars, and more.

In slightly more detail, let us begin at the beginning. At the start of time, the universe was extremely hot and ionized from the Big Bang. Over time, as space itself expanded and the gas within the universe cooled adiabatically along with that expansion, the temperature of the universe dropped low enough that the nearly uniform ionized plasma that made up the universe was able to recombine to form neutral hydrogen. This phase transition, which occurred approximately 400,000 years after the Big Bang, enabled photons to decouple from the baryonic matter, allowing photons to stream freely for the first time in the history of the universe. Those photons are what we now know as the "Cosmic Microwave Background" (CMB).

At the point of the CMB, the gravitational force had heretofore always served as second fiddle to the electromagnetic force, and the formation of structure was driven solely by dark matter (Zaroubi 2012). As such, structure had yet to form, and the release of the CMB led to a period known as the "Dark Ages" – a time when the universe had nothing to do but slowly get to work allowing slight matter over-densities grow and transform into stars, galaxies, and black holes.

So, about 100 million years passed and the universe bathed in nothing but the after-glow of the Big Bang. Finally, the first galaxies formed, and along with them bright stars to

emit ionizing radiation. Soon, we find small ionized bubbles in the intergalactic medium (IGM), the hydrogen gas filling the space between galaxies. Over time, more galaxies and their bright stars make more ionized bubbles, until eventually the entire universe's supply of loose hydrogen gas has been converted into a proton-electron ionized plasma.

This period, very creatively, is called the Epoch of Reionization – the epoch during which the universe once again became ionized, like it was at the dawn of time.

As of yet, there has been no confirmed direct detection of this time period – either of the objects that drive it nor of the gas behavior itself. This is not for lack of trying. There are currently (or soon to be) observatories looking for high-redshift galaxies and quasars (Gardner 2006), for power-spectrum measurements to find ionized regions around those high-energy objects (DeBoer 2017), and for the microscopic temperature changes in the gas of the universe (Bowman et al. 2018). As it turns out, these observations are hard to make – 13 billion light years is a long way for light to travel.

For the sake of brevity and intellectual focus, this thesis (and the experiment proposed within) will be focusing solely on observing the overall average behavior of the intergalactic medium as it evolves throughout this time period. This is referred to as the "global signal".

2.2 Overview of the Global Signal

The global signal of reionization is an observation of the overall average nature of hydrogen throughout this epoch, i.e. the spatially averaged signal from the neutral hydrogen gas, as observed using redshifted 21 cm emission from the intergalactic medium 13 billion years ago. More specifically, global signal experiments seek to observe the relationship between the gas temperature and the ambient temperature of the universe, as set by the CMB photons. By observing the evolution of the thermal gas temperature (T_K) relative to the photon temperature (T_γ), we are able to better understand how and when energy was injected into the gas (Pritchard & Loeb 2010). For example, the X-rays generated by black holes contributed to the heating of the gas, making the gas itself brighter than the ambient photons. Additionally, Lyman-α photons from Population II and III stars modify the coupling of the IGM gas temperature to the 21 cm spin temperature via the Wouthuysen-Field effect, providing a means to track early star formation (Furlanetto et al. 2006).

This signal (T_b) is measured as a function of four main variables – the thermal temperature of the hydrogen gas (T_K), the volume-averaged ionized fraction of hydrogen (x_i), the specific flux of the Lyman-α frequency (J_α), and the number density of hydrogen (n_H). One particularly convenient aspect of T_b is that its dependence on each of these quantities saturates at some point, leading to clear and separate regimes in the history of the signal that can only be described by the changes in one variable (Pritchard & Loeb 2012). These regimes can be seen in Fig. 2.1, and are physically detailed below.

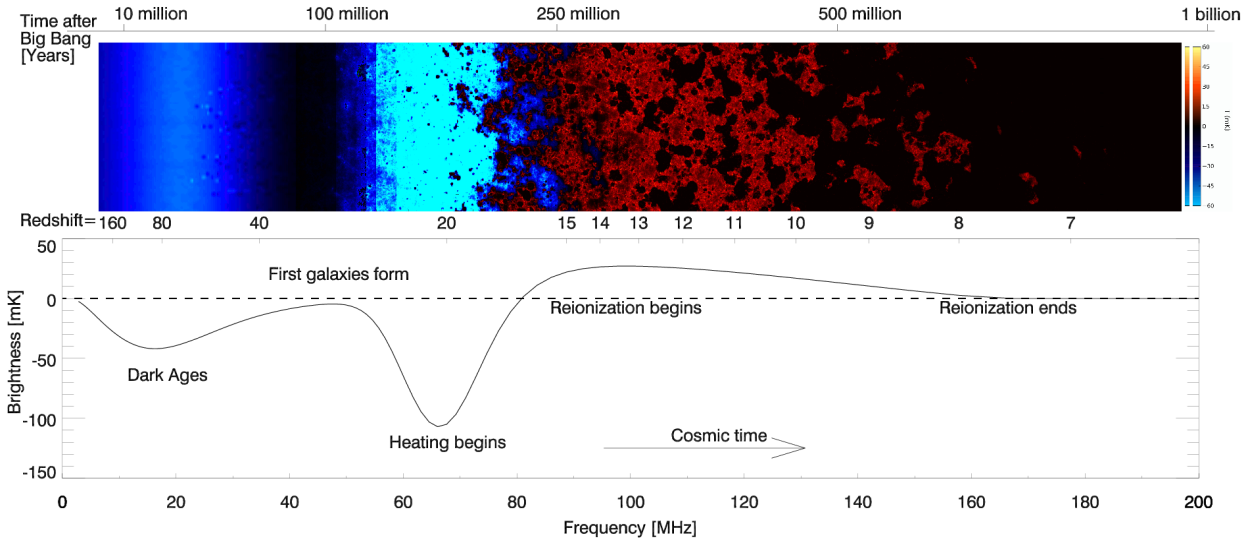

Figure 2.1: In the top half of the figure, we see a cartoon of the reionization history of the universe and the development and growth of ionized bubbles over time. In the bottom half, we see a breakdown of T_b, the brightness temperature of the 21 cm global signal, over time. There are five labeled regimes to this plot, each corresponding to the dominance of a different variable in the production of the 21 cm signal. Figure originally published in Pritchard & Loeb 2012.

Brief History of the Global Signal

- $(200 \leq z \leq 1100)$: During this time period, the residual free electron fraction remaining post-recombination and the high gas density allows the thermal and spin temperatures of the gas to remain coupled with the photon background via Compton scatting and collisional excitations. All temperatures are the same, and therefore there will be no detectable 21 cm signal.

- $(40 \leq z \leq 200)$: As cosmological expansion continues, Compton scattering no longer couples the thermal temperature of the gas to the CMB photons, and the gas and radiation decouple and go out of equilibrium. Collisional coupling sets the spin temperature $T_S < T_\gamma$, leading to an absorption feature in the 21 cm global signal.

- $(30 \leq z \leq 40)$: Expansion continues and collisional interactions are no longer effective at coupling the thermal and spin temperatures of the gas. The excitation levels shift to being set by radiative coupling to the CMB, such that $T_S = T_\gamma$, and there is no detectable 21 cm signal.

- $(15 \leq z \leq 30)$: As the first sources (e.g. stars, active galactic nuclei (AGN), etc...) ignite, they begin emitting high energy Lyman-α and X-ray photons. The hyperfine

populations couple to the thermal temperature of the cold gas via the Wouthuysen-Field effect, such that $T_S \sim T_K < T_\gamma$, resulting in an absorption feature in the 21 cm global signal.

– ($7 \leq z \leq 15$): The radiation (particularly the X-rays) from bright sources heat the gas, $T_K > T_\gamma$ and we see 21 cm emission in the global signal. Lyman-α coupling is still effective at setting the level populations.

– ($z \leq 7$): Enough ionizing radiation has spread throughout the universe that the IGM has been converted from neutral to ionized, and reionization is complete.

Chapter 3

Interferometry

3.1 Brief Overview

The Flat Sky Approximation and Its Limitations

3.2 Spatial Modes and Interferometric Sensitivities

Spatial Fourier Transforms

3.3 Observing the Spatial Monopole with an Interferometer

Chapter 4

Absorber – A New Approach to Monopole Interferometry

4.1 Practical Instrumentation

4.2 Manipulating the Spatial Monopole

4.3 Initial Results

Chapter 5

Overview of the Theory of HYPERION

5.1 Simulation

The basis of our simulation lies in the calculation of a visibility using Eq. (5.1).

$$V(u,v) = \int A(\hat{s}) \cdot T_{sky}(\hat{s})\ e^{-2\pi i \frac{\vec{b}\cdot\hat{s}}{\lambda}} d\Omega \tag{5.1}$$

From this equation, we have three parameter spaces to play in: the beam of the antenna $A(\hat{s})$, the brightness and spatial behavior of the sky $T_{sky}(\hat{s})$, and the baseline vector $\vec{b}$. For ease of organization, we'll now split our discussion into two parts, sky characteristics vs. system characteristics.

Sky Characteristics & Parameters

At present, our goal is to better understand how an interferometer receives signal from a monopole sky, so we're only considering skies without any spatial variation. However, while we are only inputting spatially flat maps into the simulation, spectral variation across our science band is an open variable that we consider. The simulation has functions for both spectrally-flat (for calibration and verification purposes) and synchrotron-characteristic sky maps, using Eq. (5.2) as our basis for calculating brightness temperature as a function of frequency.

$$T(\nu) = T(\nu_{150})\Big(\frac{\nu}{\nu_{150}}\Big)^{-\beta} \tag{5.2}$$

System Characteristics & Parameters

This leads us to the characteristics of our interferometer itself. Within this framework, there are two key areas of interest to us: how our sensitivity to the monopole varies with the separation between antennas, and how it changes in the presence of different absorber structures and materials. Another way of viewing it would be: how do the characteristics of the individual elements and of the array design affect our ability to make this measurement.

Let us first consider the array design, i.e. baseline separations. For this simulation, we import a model array using the AIPy AntennaArray framework, which enables us to carry around an array with known geometry and baseline separations, along with individual antenna beam patterns and accessible frequencies. With this information and the previously made sky maps, we are now able to calculate our visibilities across many frequencies by using Eq. (5.1).

Intuitively, we expect that the sensitivity to the global signal will be maximized with the smallest baseline separations, which correspond to a position in the *uv*-plane close to the origin, or the zero-spacing mode. The trade-off of this, from a design perspective, comes in the difficulty of ameliorating cross-talk in a densely packed array. We want to optimize our array design to space our antennas as loosely as possible while also maintaining workable sensitivity to the monopole term, as this will best enable us to mitigate systemic problems in our instrument and perform a successful experiment.

The AntennaArray framework also enables us to carry around models of the beams of the antennas, which is a convenient way to import absorbers into the simulation. Essentially, within the context of the simulation, the absorbers act as a modification term on the beam pattern, changing the way that each individual antenna sees the sky. This works as follows:

To start, we need a beam. HYPERION uses SARAS-style fat dipole antennas in our instrument, which means we will be using a frequency-invariant dipole beam pattern in our simulation to match (Patra et al. 2013). This is the base beam model used throughout the simulation, calculated using Eq. (5.3).

$$A(\theta, \phi, \nu) = \cos\left(\frac{\frac{\pi}{2}\cos\theta}{\sin\theta}\right) \tag{5.3}$$

The next step is to add the absorber, which we do via modification of the AIPy Antenna beam. The absorber structure in our simulation is essentially a cylindrical wall of uniform height centered around each antenna, so that the antenna sees a rotationally symmetric structure. The parameters we can play with are the absorptivity of the material (i.e. how much attenuation does the absorber provide at each frequency), the height of the absorber walls, and how smooth the transition from absorber to sky is. This calculation is done using Eq. (5.4),

$$B(\theta, \phi, \nu) = \left[10^{\alpha(\nu)/20}\left(\frac{1}{2} + \frac{1}{2}\tanh\left(\frac{\theta - (\frac{1}{2} - \theta_0)}{a}\right)\right) + \left(1 - \left(\frac{1}{2} + \frac{1}{2}\tanh\left(\frac{\theta - (\frac{1}{2} - \theta_0)}{a}\right)\right)\right)\right] \tag{5.4}$$

where $\alpha(\nu)$ is the absorptivity by frequency of the absorber, θ_0 is the cutoff angle of the structure (i.e. θ_0 is the height of the absorber walls), and a is the smoothing parameter that blends the transition between the absorber and the sky.

This term is then combined with the Antenna beam, giving us Eq. (5.5).

$$A'(\theta, \phi, \nu) = A(\theta, \phi, \nu)B(\theta, \phi, \nu) \tag{5.5}$$

Calculating Visibilities by Baseline Separation

One of the fundamental constructs of the theory of astronomical interferometry is that samples spatial variance on the sky. Interferometers, by nature, are not designed to observe global light sources. Rather, interferometers excel at observing differences – a star or other point source will have light in one place and no light everywhere else, galaxies will have clumpy, fluffy light in some places but not all places. The interferometer can be built and designed to observe some scales better than others, and can tease out these differential light sources with great success.

So one might reasonably be surprised to hear that we are taking an interferometer and trying to do the one exact thing that it is, theoretically, unequipped to handle: trying to observe a global average phenomenon on the sky.

Chapter 6

Sensitivity to the Monopole Sky

6.1 Simulated

lay out the case that absorber helps us maximize interferometric sensitivity to monopole, lay out the case that we can use the characteristics of this sensitivity to potentially help us pick out monopole vs. higher order terms (some kind of filtering around sensitivity vs. u mode)

As can be easily seen in Figures 6.1 and 6.2, all interferometers have a non-zero sensitivity to the monopole mode of the sky. As the number of wavelengths of separations increases, that sensitivity also quickly evaporates.

now speak to absorbers that we tried and how they all performed. show results of monopole sky with absorber, compare to without absorber and show that there is greater sensitivity

We can also begin to see a characteristic shape of the sensitivity in the uv-plane, with peaks and nulls placed at regular intervals in uv-space. The predictability of this shape could allow us to use it as a calibration tool, if properly understood. In particular, it could be a valuable way to remove leakage from non-monopole terms into our signal. Given that this characteristic shape derives only from the monopole sky and the shape of the beam, we know that any observational deviations in this shape must come from the sky rather than the system. Therefore, it may be possible to use this information as a way to

Additionally, this shape enables us to do some weighting of our observational data. By knowing exactly what modes we expect to see the monopole term at its brightest and dimmest, we can properly weight and interpret our data at each mode and frequency, enabling us to better compare data points at different points in uv-space and frequency.

6.2 Recovered

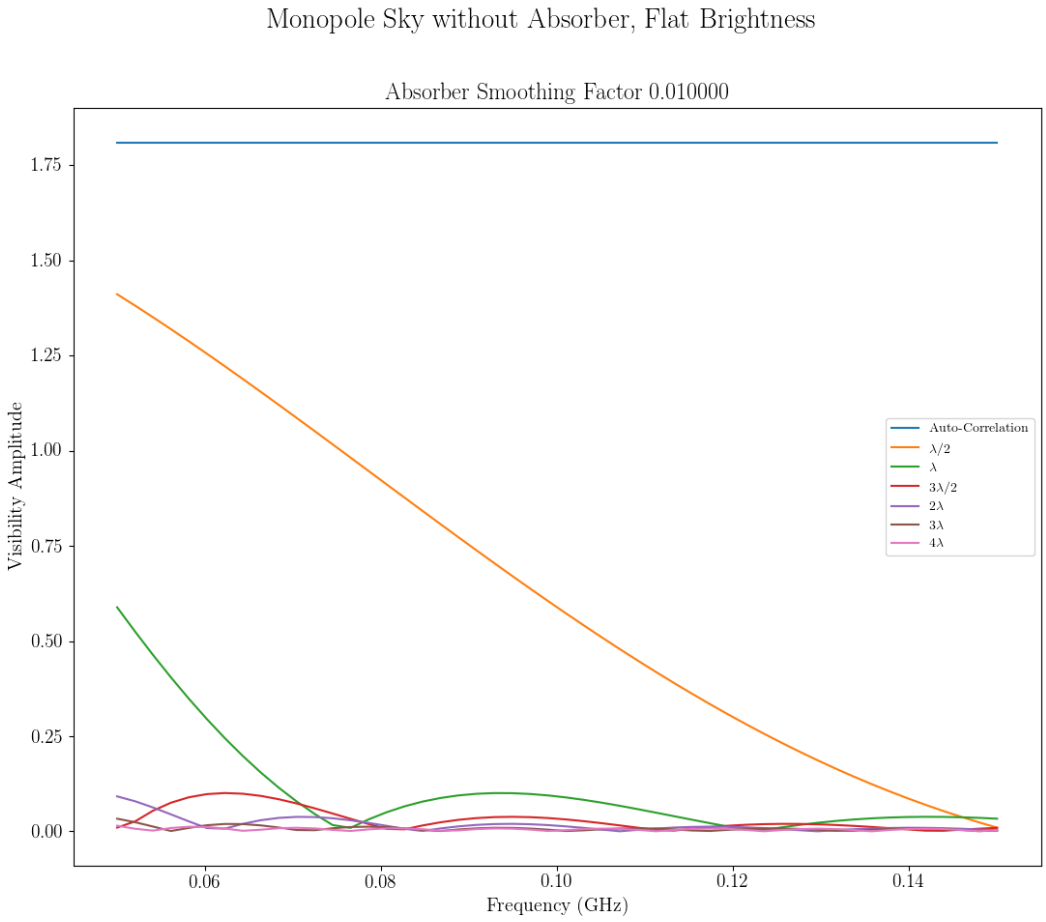

Figure 6.1: Shown here is the absolute value of the visibility of a spectrally flat monopole sky with no absorber walls versus frequency. As can be seen already, the interferometer does have non-zero sensitivity to the monopole, though it is plainly clear that the autocorrelation term (shown in blue) is more sensitive than any of the non-zero interferometric baseline pairings.

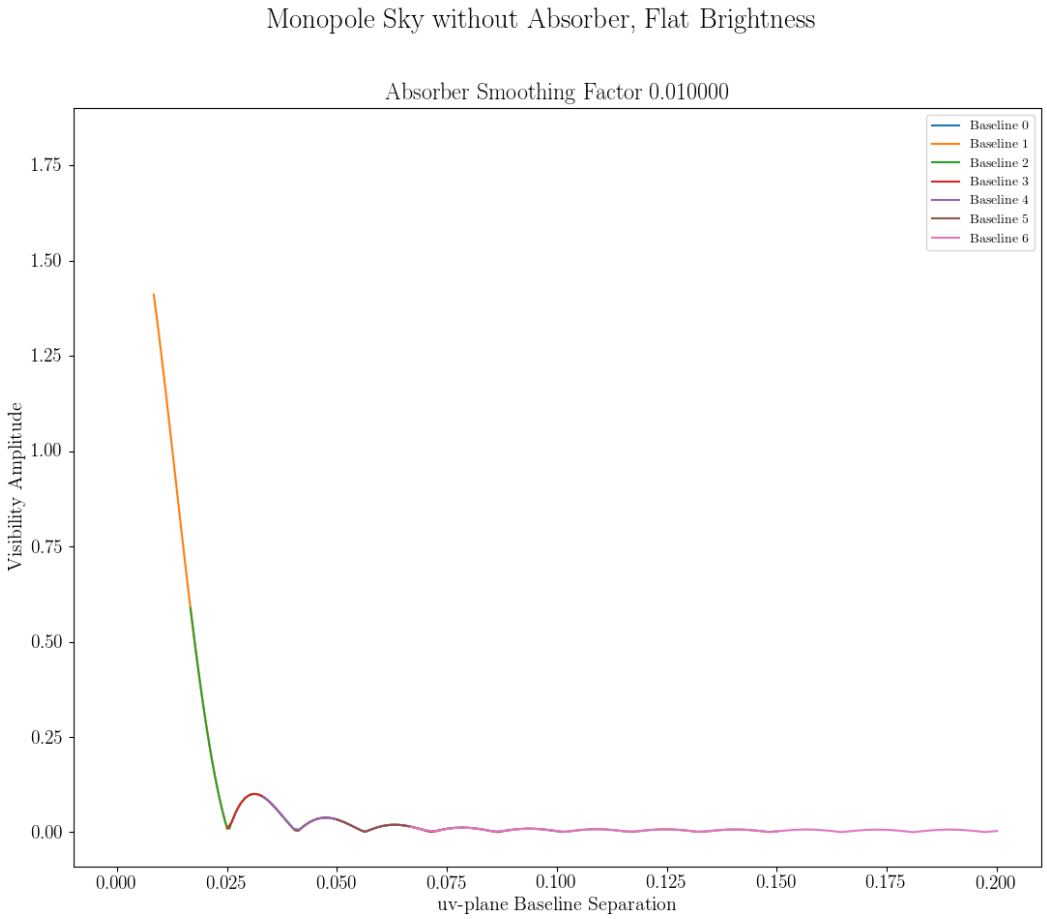

Figure 6.2: REMAKE THIS FIGURE Shown here is the absolute value of the visibility of a spectrally flat monopole sky with no absorber walls versus uv-baseline. As can be seen already, the interferometer has a non-zero sensitivity to the monopole at non-zero baseline separations.

Chapter 7

Conclusion

review all chapters and results, but pithier

Bibliography

Bowman, J. D., Rogers, A. E. E., Monsalve, R. A., Mozdzen, T. J., & Mahesh, N. 2018, Nature, 555

DeBoer, D. R. e. a. 2017, Publications of the Astronomical Society of the Pacific, 129

Furlanetto, S. R., Oh, S. P., & Briggs, F. H. 2006, Physics Report, 433

Gardner, J. P. e. a. 2006, Space Science Reviews, 123

Kundert, K. 2016, The Relationship Between System Temperature and Sky Beam Coverage, Memo 1, HYPERION

Patra, N., Subrahmanyan, R., Raghunathan, A., & Shankar, N. U. 2013, Experimental Astronomy, 36

Pritchard, J. R., & Loeb, A. 2010, Physical Review D, 82

—. 2012, Reports on Progress in Physics, 75

Zaroubi, S. 2012, in The First Galaxies, – Theoretical Predictions and Observational Clues, ed. T. Wiklind, B. Mobasher, & V. Bromm (Springer), 45–101